Supporting Information

Morphological and isotopic changes of heterocystous cyanobacteria in response to N_2 partial pressure

Silverman, Kopf, Bebout, Gordon, Som

Appendix S1: Data processing

All data (in Excel format) and source code (in R Markdown format) used to produce the figures, data tables and analyses for this paper are available online at www.github.com/KopfLab/2018_Silverman_et_al. Rendered versions of the source code are available at 2018_Silverman_et_al.kopflab.org.

Appendix S2: Heterocyst spacing

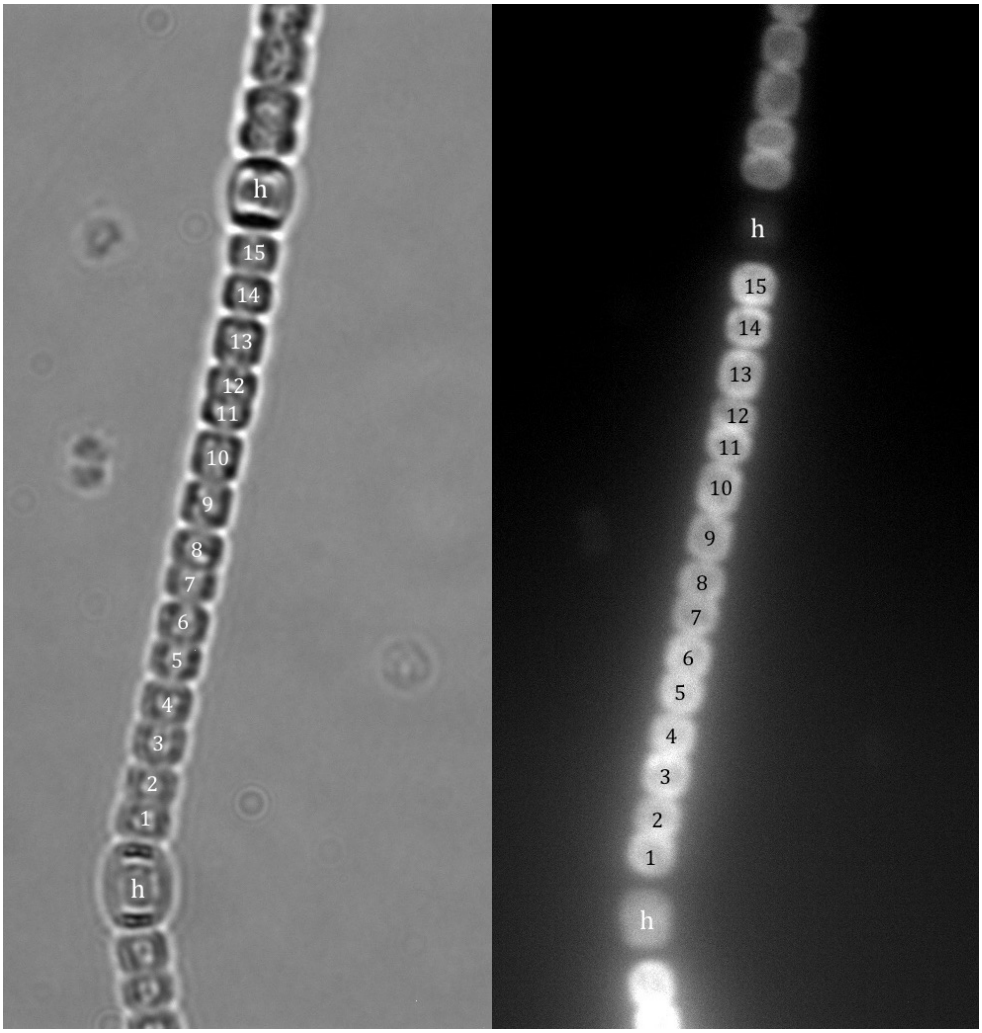

Figure S1: Example of heterocyst interval measurements. Bright-field and fluorescence micrographs of *Anabaena* filaments were used in tandem to identify heterocysts and count the number of vegetative cells (n_{cbh}= 15 here) between neighboring heterocysts (h).

Fig. S1 illustrates an example of how the heterocyst distances in all conditions were quantified. Tables S1 and S3 summarize the data represented in Figs. 4 and S2 for *A. cylindrica* and *A. variabilis*, respectively. Measurements of stationary phase heterocyst distance (n_{cbh}, number of vegetative cells between heterocysts) for each pN_2 are reported alongside the total number of heterocyst intervals counted (i.e., individual segments between two heterocysts), as well as bootstrap estimates (1000 resampled distributions) of the mean ($\bar{n}_{\mathrm{cbh}}$) and median (M_{cbh}) distances with their respective standard errors (± 1 SE). Tables S2 and S4 summarize the bootstrap (1000 resamples) estimated differences (± 1 SE) and significance in heterocyst distance ($\Delta\bar{n}_{\mathrm{cbh}}$) between the different experimental conditions. Reported significance levels are based on the t-test statistic of the bootstrapped distribution differences (p-value < 0.001 = ***; p-value < 0.01 = **; p-value < 0.05 = *; no significant difference: -). Using a non-parametric Wilcoxon–Mann–Whitney test on the observed distances instead of bootstrap comparisons provided identical significance levels (with p-values even slightly lower). The results show that heterocyst distances in *A. cylindrica* were significantly shorter in filaments cultivated at lower N_2 partial pressures than at higher pN_2 (i.e., p-value < 0.01 for all combinations, Table S2) while only the $pN_2 = 0$ bar condition showed significantly shorter heterocyst distances for *A. variabilis* (i.e., all comparisons but the first column and first row of Table S4 do not show any statistically significant differences). Fig. S3 provides a comparison between the stationary phase data to other growth phases for *A. cylindrica* as described in the figure caption.

Table S1: Summary statistics of *A. cylindrica* heterocyst distances by culture growth phase in response to N_2 partial pressure. Reported errors are bootstrapped standard errors (± 1 SE).

	pN_2 [bar]	segments [#]	$\bar{n}_{\mathrm{cbh}}$ [# cells]	M_{cbh} [# cells]
early-exponential	0.0	-	-	-
	0.1	643	9.33 ± 0.17	9.00 ± 0.48
	0.3	457	9.42 ± 0.20	9.00 ± 0.46
	0.5	431	11.56 ± 0.25	12.00 ± 0.54
	0.8	483	12.87 ± 0.27	12.00 ± 0.50
late-exponential	0.0	123	7.70 ± 0.31	7.00 ± 0.49
	0.1	338	11.07 ± 0.29	11.00 ± 0.40
	0.3	298	12.70 ± 0.29	12.00 ± 0.49
	0.5	370	13.87 ± 0.28	14.00 ± 0.47
	0.8	250	16.27 ± 0.47	15.00 ± 0.55
stationary	0.0	412	8.10 ± 0.18	8.00 ± 0.05
	0.1	762	10.62 ± 0.19	10.00 ± 0.48
	0.3	377	14.85 ± 0.29	14.00 ± 0.46
	0.5	250	16.94 ± 0.42	16.00 ± 0.44
	0.8	321	19.17 ± 0.45	18.00 ± 0.72

Table S2: Summary of the differences and significance in heterocyst distance ($\Delta\bar{n}_{\mathrm{cbh}}$) at different N_2 partial pressures for *A. cylindrica* in late-exponential growth phase. Reported errors are bootstrapped standard errors (± 1 SE).

$\Delta\bar{n}_{\mathrm{cbh}}$	0.0 bar	0.1 bar	0.3 bar	0.5 bar	0.8 bar
0.0 bar	-	3.36 ± 0.42 (***)	4.98 ± 0.43 (***)	6.17 ± 0.42 (***)	8.56 ± 0.57 (***)
0.1 bar	-3.36 ± 0.42 (***)	-	1.61 ± 0.41 (***)	2.81 ± 0.40 (***)	5.19 ± 0.57 (***)
0.3 bar	-4.98 ± 0.43 (***)	-1.61 ± 0.41 (***)	-	1.20 ± 0.41 (**)	3.58 ± 0.55 (***)
0.5 bar	-6.17 ± 0.42 (***)	-2.81 ± 0.40 (***)	-1.20 ± 0.41 (**)	-	2.38 ± 0.54 (***)
0.8 bar	-8.56 ± 0.57 (***)	-5.19 ± 0.57 (***)	-3.58 ± 0.55 (***)	-2.38 ± 0.54 (***)	-

Table S3: Summary statistics of *A. variabilis* heterocyst distances in late-exponential growth phase in response to N_2 partial pressure. Reported errors are bootstrapped standard errors (±1 SE).

pN_2 [bar]	segments [#]	$\bar{n}_{cbh}$ [# cells]	M_{cbh} [# cells]
0.0	101	20.6 ± 1.1	21.0 ± 1.4
0.1	64	27.4 ± 2.2	25.0 ± 3.1
0.3	78	27.1 ± 1.7	26.0 ± 1.4
0.5	82	23.7 ± 1.6	23.5 ± 2.0
0.8	92	26.6 ± 1.5	26.5 ± 1.8

Table S4: Summary of the differences and significance in heterocyst distance ($\Delta\bar{n}_{cbh}$) at different N_2 partial pressures for *A. variabilis* in exponential growth phase. Reported errors are bootstrapped standard errors (±1 SE).

$\Delta\bar{n}_{cbh}$	0.0 bar	0.1 bar	0.3 bar	0.5 bar	0.8 bar
0.0 bar	-	6.8 ± 2.5 (*)	6.5 ± 2.0 (**)	3.2 ± 1.9 (-)	6.1 ± 1.9 (**)
0.1 bar	-6.8 ± 2.5 (*)	-	-0.3 ± 2.8 (-)	-3.7 ± 2.7 (-)	-0.7 ± 2.6 (-)
0.3 bar	-6.5 ± 2.0 (**)	0.3 ± 2.8 (-)	-	-3.4 ± 2.34 (-)	-0.4 ± 2.3 (-)
0.5 bar	-3.2 ± 1.9 (-)	3.7 ± 2.7 (-)	3.4 ± 2.4 (-)	-	3.0 ± 2.2 (-)
0.8 bar	-6.2 ± 1.9 (**)	0.7 ± 2.6 (-)	0.4 ± 2.3 (-)	-3.0 ± 2.2 (-)	-

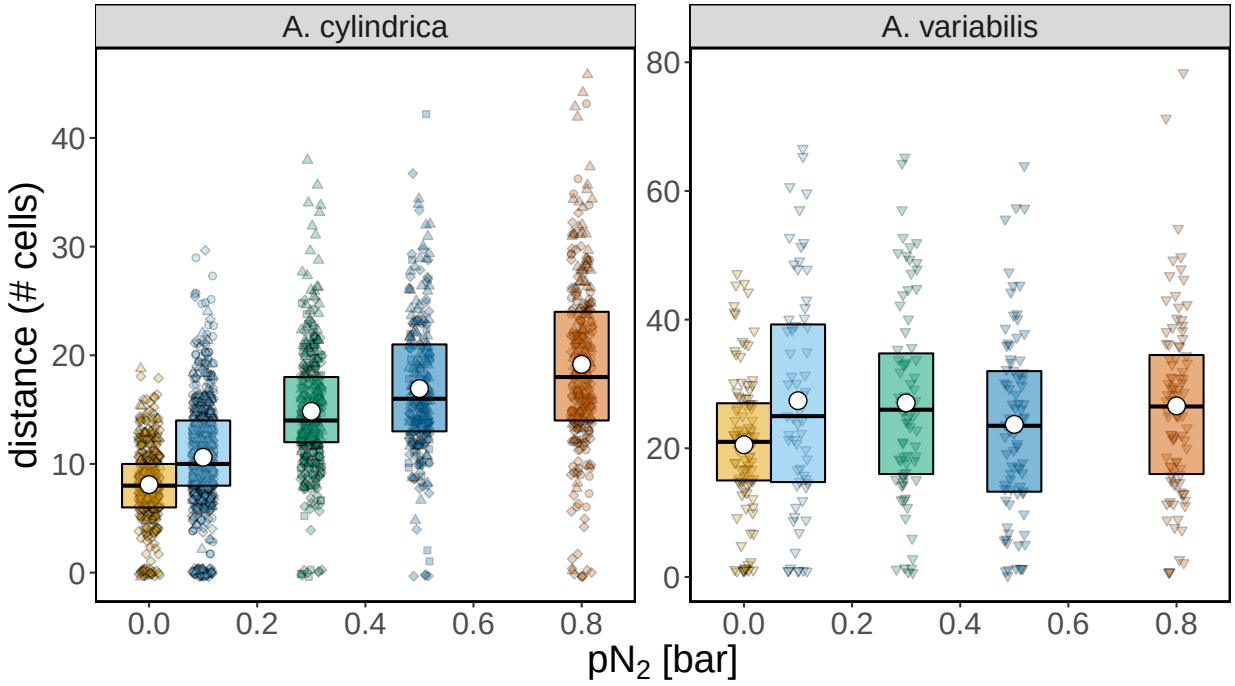

Figure S2: Exponential phase heterocyst distances in response to pN_2 for *A. cylindrica* and *A. variabilis*. Cultures were induced to develop heterocysts in nitrogen-free BG-11_0 media under different N_2 partial pressures, and heterocyst distances were measured in exponential phase by microscopy. Each recorded heterocyst distance is represented by an individual data point; symbols distinguish individual experiments conducted. The distribution of heterocyst distances for each pN_2 is shown as a box plot with the mean (circle), median (center line), and 50% interquartile range (box height). These data are summarized with the bootstrapped means and error of the means in the main text (Fig. 4).

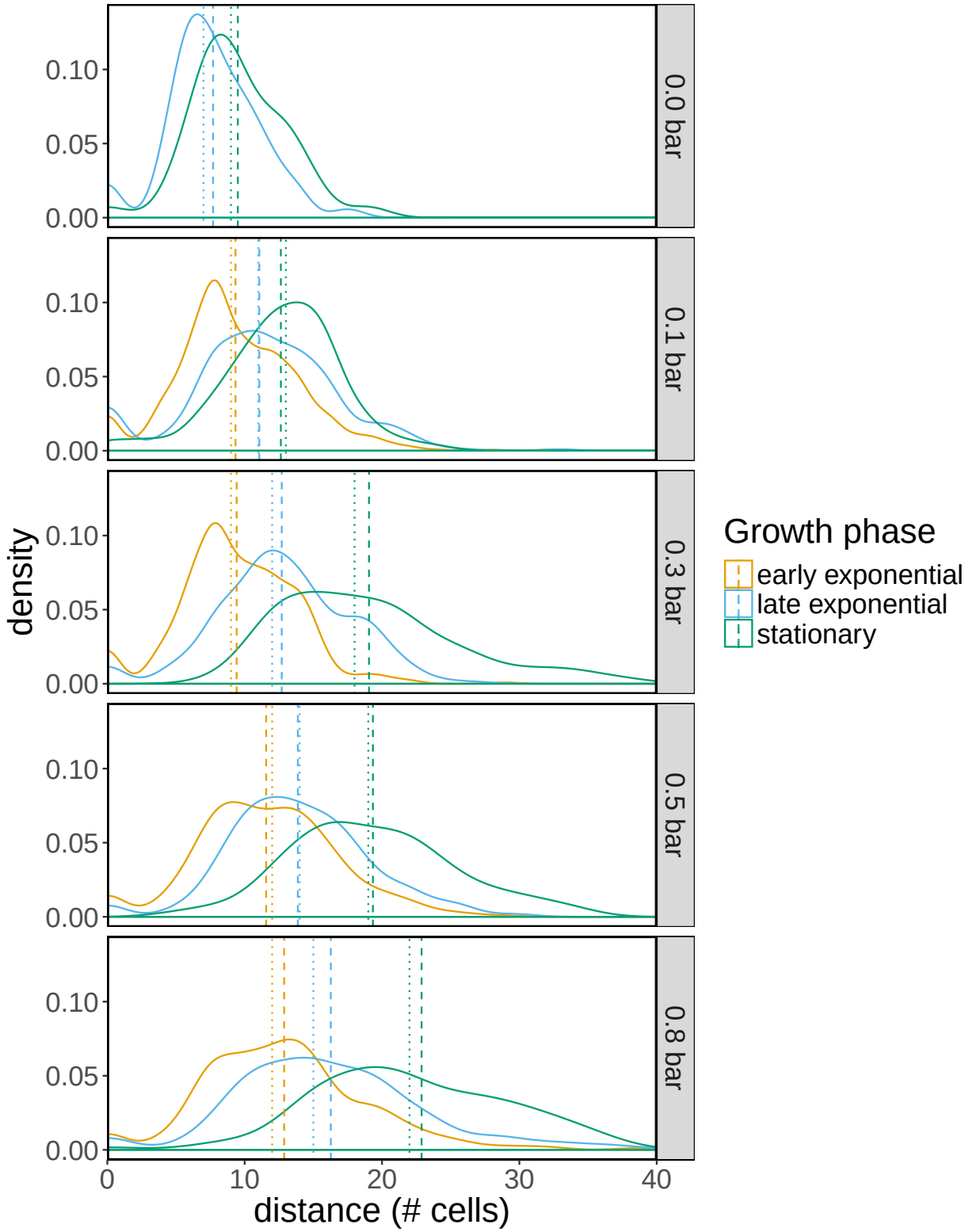

Figure S3: Comparison of heterocyst distances at different growth phases of *Anabaena cylindrica*. Cultures were induced to develop heterocysts in nitrogen-free BG-11_0 media under different N_2 partial pressures and were sampled at t=4 d (early-exponential phase), 7 d (late-exponential phase) and 15 d (stationary phase). See growth curves in Fig. S5 for corresponding optical densities. Heterocyst distances were measured by microscopy and are visualized here as density curves. In descending vertical order of the panels: pN_2 = 0, 0.1, 0.3, 0.5 and 0.8 bar. Despite biological variation in the different growth phases, the mean (dashed lines) and median (dotted lines) heterocyst distances increased with pN_2 at all three time points.

Appendix S3: Growth curves and growth rate estimates

A. cylindrica cultures were grown in nitrate-containing BG-11 under two different N_2 partial pressures and showed nearly identical growth (Fig. S4), indicating pN_2 does not affect culture growth when the cells are not fixing N_2. In contrast, the growth patterns of *A. cylindrica* and *A. variabilis* were significantly affected by pN_2 (Fig. S5). Optical density data was assumed to be most reliable as a relative proxy for biomass at OD_{750} values up to 0.4 (a conservative upper limit for the linearity of optical density measurements) as indicated by the black horizontal lines in Fig. S5. Maximum growth rates (μ) were estimated from the OD_{750} data in this interval with a log-linear regression model (vs. time t) based on the following equations:

- Exponential growth equation for biomass (B): $B(t) = B_{t0} \cdot e^{\mu t}$
- Linear relationship between OD_{750} and biomass with some proportionality factor k: $\mathrm{OD}_{750} = k \cdot B$
- Resulting linear regression model: $\ln\left(\frac{B(t)}{B_0}\right) = \mu \cdot t \rightarrow \ln\left(\frac{\mathrm{OD}_{750}(t)}{\mathrm{OD}_{750}(t_0)}\right) = \mu \cdot t$

The calculated growth rates (slopes of the regression) were bootstrapped with 1000 resamplings of the original OD data to estimate mean growth rates and standard errors for each experimental condition. Fig. S6 summarizes the growth rates showing that both species of *Anabaena* grew more slowly at $pN_2 < 0.5$ bar but showed no statistically significant growth inhibition at 0.5 bar and above. These growth rate data were used in the isotope fractionation and enzyme kinetic models presented in Appendix S5: and Appendix S6:.

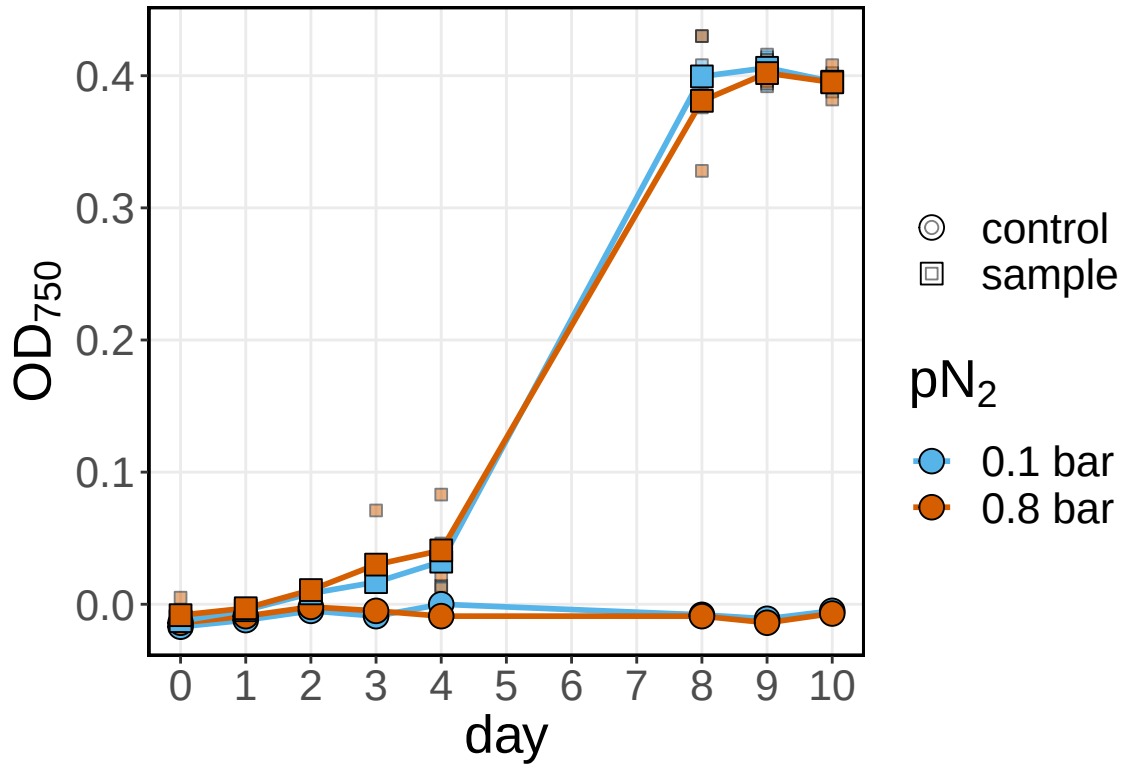

Figure S4: Optical density at 750 nm (OD_{750}) of *Anabaena cylindrica* grown in nitrate-rich BG-11 under 0.1 and 0.8 bar N_2. In absence of nitrogen-fixing conditions, culture growth is not affected by pN_2.

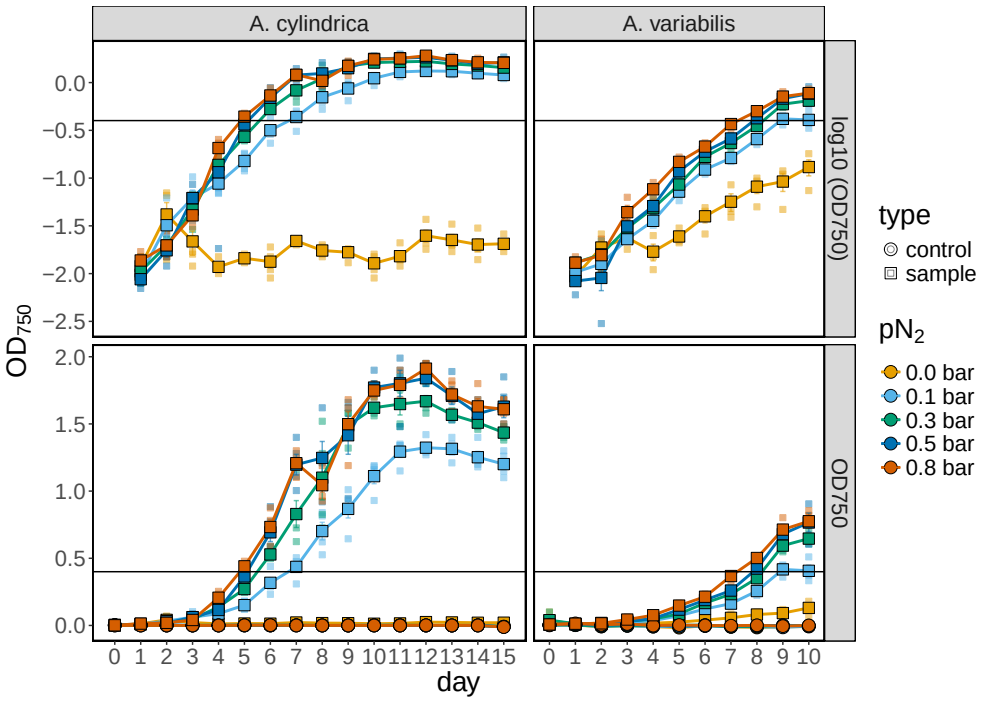

Figure S5: Optical density at 750 nm (OD_{750}) of *Anabaena* sp. grown in BG-11_0 under different pN_2 conditions. Top panels show OD_{750} on logarithmic scale, bottom panels on linear scale. Lines connect bootstrapped averages of biological replicates with smaller symbols showing individual data points. Errors bars are bootstrapped standard errors ($\pm$1 SE) and may be smaller than symbol sizes. Black horizontal lines show optical density cutoff (OD_{750}= 0.4) for growth rate calculations.

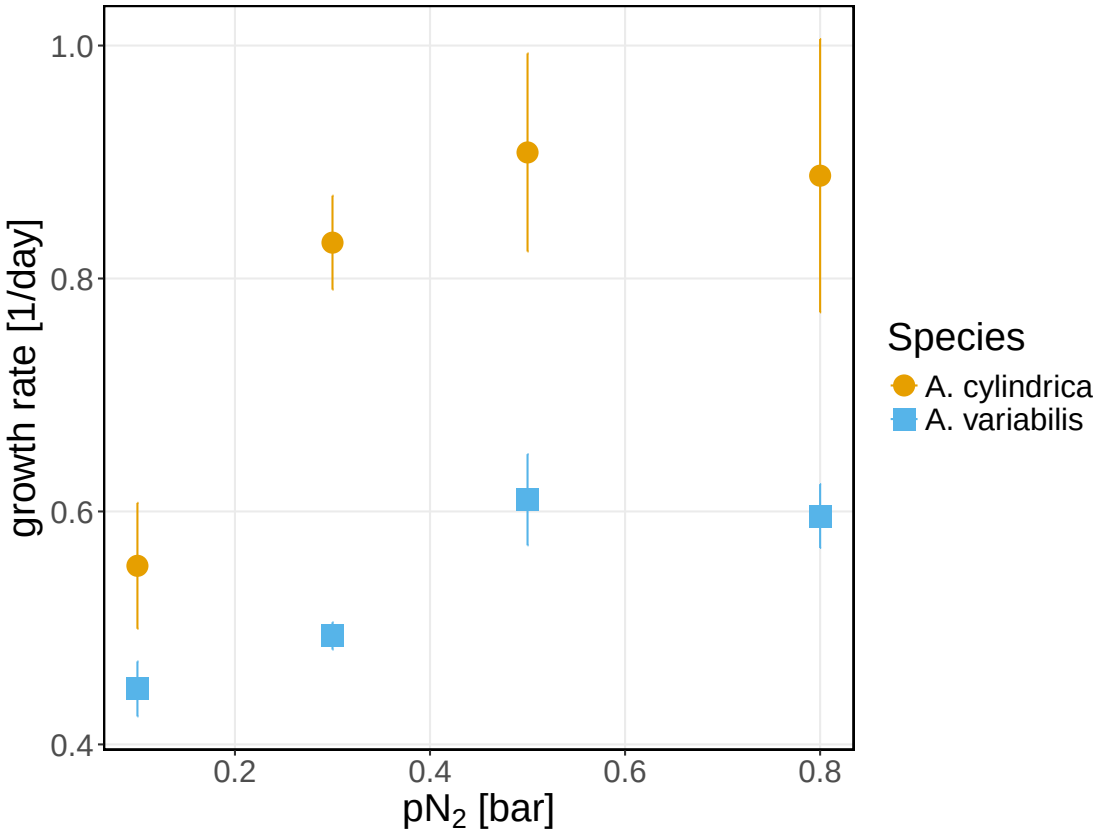

Figure S6: Growth rates of *Anabaena cylindrica* (circles) and *Anabaena variabilis* (squares) grown under different pN_2 conditions. Data points are bootstrapped averages based on regression analyses of the data from initial log phases of the growth curves in Fig. S5. Errors bars are bootstrapped standard errors ($\pm$1 SE).

Appendix S4: Experimental pH, O_2 and CO_2 variation

Preliminary growth experiments were carried out to test the growth yield, and pH and O_2 variations of *A. cylindrica* with the total inorganic carbon available from one flushing of the headspace. The experimental system in this study consists of 25 ml anaerobic culture tubes with 10 ml of medium initially adjusted to a pH of 7.8 in the presence of 20 mM HEPES (pKa = 7.5), and 15 ml of headspace under atmospheric CO_2 conditions (~400 ppm) at room temperature. Upon quick flushing of the headspace with different gas mixtures that contain 0.2 bar CO_2, the total inorganic carbon is increased, which leads to a decrease in pH. As the inorganic carbon is consumed through photosynthetic activity, the pH increases again. Efficient equilibration between the headspace and liquid during growth is achieved by continuous agitation.

The available carbon from one headspace sparging enabled the cultures to grow to an optical density of ~0.4 (panel A in Fig. S7). Inorganic carbon and pH are calculated for these preliminary experiments based on carbonate chemistry, with general equilibrium equations of the carbonate system as follows (assuming STP):

$$\text{dissociation of carbonic acid: } \mathrm{H_2CO_3^*} \rightleftharpoons \mathrm{H^+ + HCO_3^-}$$

$$\text{with dissociation constant } \frac{[\mathrm{H^+}][\mathrm{HCO_3^-}]}{[\mathrm{H_2CO_3^*}]} = K_1 = 10^{-6.3}$$

$$\text{dissociation of bicarbonate: } \mathrm{HCO_3^-} \rightleftharpoons \mathrm{H^+ + CO_3^{2-}}$$

$$\text{with dissociation constant } \frac{[\mathrm{H^+}][\mathrm{CO_3^{2-}}]}{[\mathrm{HCO_3^-}]} = K_2 = 10^{-10.3}$$

$$\text{water dissociation: } \mathrm{H_2O} \rightleftharpoons \mathrm{H^+ + OH^-}$$

$$\text{with dissociation constant } [\mathrm{H^+}][\mathrm{OH^-}] = K_\mathrm{w} = 10^{-14}$$

$$\text{dissolved inorganic carbon (DIC): } [\mathrm{DIC}] = [\mathrm{H_2CO_3^*}] + [\mathrm{HCO_3^-}] + [\mathrm{CO_3^{2-}}]$$

$$\text{charge balance (not considering any other solutes): } [\mathrm{H^+}] - [\mathrm{HCO_3^-}] - 2\cdot[\mathrm{CO_3^{2-}}] - [\mathrm{OH^-}] = 0$$

Besides the carbonate system, both the basicity from the addition of sodium hydroxide (adding $[\mathrm{Na^+}]$ and $[\mathrm{OH^-}]$ during initial pH adjustment) and any dissociated pH buffer (here the portion of the total HEPES, $[A_\mathrm{T}]$ for short, that is dissociated into $[\mathrm{A^-}]$ and $[\mathrm{H^+}]$ with acid dissociation constant $K_\mathrm{a} = \frac{[\mathrm{A^-}][\mathrm{H^+}]}{[\mathrm{AH}]}$ and mass balance $[A_\mathrm{T}] = [\mathrm{AH}] + [\mathrm{A^-}]$) contribute to the overall charge balance (note that the second dissociation of HEPES around pH 3 is not significant at the circumneutral pHs considered here and thus omitted for clarity):

$$[\mathrm{H^+}] - [\mathrm{HCO_3^-}] - 2\cdot[\mathrm{HCO_3^{2-}}] - [\mathrm{OH^-}] - [\mathrm{A^-}] + [\mathrm{Na^+}] = 0$$

CO_2 is moderately soluble in water forming aqueous CO_2 and hydrated carbonic acid with a Henry's law constant of $K_\mathrm{H} = 3.3 \cdot 10^{-4} \frac{\mathrm{mol}}{\mathrm{m^3 Pa}} = 0.033 \frac{\mathrm{M}}{\mathrm{atm}}$ at $\mathrm{T} = 298.15\mathrm{K}$ (25°C). Substituting in all relevant acid dissociation and gas dissolution constants (K_x) yields the following equation:

$$[\mathrm{H^+}] + [\mathrm{Na^+}] - \frac{K_\mathrm{a}\cdot[A_\mathrm{T}]}{K_\mathrm{a} + [\mathrm{H^+}]} - \frac{K_1 K_\mathrm{H}\cdot\mathrm{pCO_2}}{[\mathrm{H^+}]} - 2\frac{K_1 K_2 K_\mathrm{H}\cdot\mathrm{pCO_2}}{[\mathrm{H^+}]^2} - \frac{K_\mathrm{w}}{[\mathrm{H^+}]} = 0$$

where K_H is Henry's law constant. For a closed system such as the one used in this study (stoppered culture tubes), the mass balance based on total moles of carbon in the entire system provides an additional constraint.

Total inorganic carbon (C_{T}) can be mass balanced using the ideal gas law and relevant acid dissociation and gas dissolution constants:

$$C_{\mathrm{T}} = n_{\mathrm{CO_2}(g)} + V_{\mathrm{liquid}} \cdot \mathrm{DIC}$$

$$\mathrm{DIC} = [\mathrm{H_2CO_3^*}] + [\mathrm{HCO_3^-}] + [\mathrm{CO_3^{2-}}] = K_{\mathrm{H}} \cdot \mathrm{pCO_2} \left(1 + \frac{K_1}{[\mathrm{H^+}]} + \frac{K_1 K_2}{[\mathrm{H^+}]^2}\right)$$

$$n_{\mathrm{CO_2(g)}} = \frac{\mathrm{pCO_2} \cdot V_{\mathrm{headspace}}}{\mathrm{RT}}$$

$$C_{\mathrm{T}} = \mathrm{pCO_2} \cdot \left[\frac{V_{\mathrm{headspace}}}{\mathrm{RT}} + V_{\mathrm{liquid}} \cdot K_{\mathrm{H}} \left(1 + \frac{K_1}{[\mathrm{H^+}]} + \frac{K_1 K_2}{[\mathrm{H^+}]^2}\right)\right]$$

With these constraints, a final equation relating pH to the added base $[\mathrm{Na^+}]$, total buffer $[A_{\mathrm{T}}]$, total inorganic carbon (C_{T}) and headspace + liquid volume in the system can be derived and solved for pH by standard numerical root-finding algorithms.

$$[\mathrm{H^+}] + [\mathrm{Na^+}] - \frac{K_{\mathrm{a}}}{K_{\mathrm{a}} + [\mathrm{H^+}]} \cdot [A_{\mathrm{T}}] - \frac{\frac{K_1}{[\mathrm{H^+}]} + 2\frac{K_1 K_2}{[\mathrm{H^+}]^2}}{\frac{V_{\mathrm{headspace}}}{K_{\mathrm{H}} \cdot \mathrm{RT}} + \left(1 + \frac{K_1}{[\mathrm{H^+}]} + \frac{K_1 K_2}{[\mathrm{H^+}]^2}\right) V_{\mathrm{liquid}}} \cdot C_{\mathrm{T}} - \frac{K_{\mathrm{w}}}{[\mathrm{H^+}]}$$

$$10^{-\mathrm{pH}} + [\mathrm{Na^+}] - \frac{1}{1 + 10^{(\mathrm{p}K_a - \mathrm{pH})}} \cdot [A_{\mathrm{T}}] - \frac{10^{(\mathrm{pH} - \mathrm{p}K_1)} + 2 \cdot 10^{(2 \cdot \mathrm{pH} - \mathrm{p}K_1 - \mathrm{p}K_2)}}{\frac{V_{\mathrm{headspace}}}{K_{\mathrm{H}} \cdot \mathrm{RT}} + (1 + 10^{(\mathrm{pH} - \mathrm{p}K_1)} + 10^{(2 \cdot \mathrm{pH} - \mathrm{p}K_1 - \mathrm{p}K_2)}) V_{\mathrm{liquid}}} \cdot C_{\mathrm{T}} - 10^{(\mathrm{pH} - \mathrm{p}K_{\mathrm{w}})} = 0$$

In parallel to the pH increase as during inorganic carbon consumption through photosynthesis, molecular oxygen ($\mathrm{O_2}$) is produced with the 1:1 stoichiometry of photosynthesis ($\mathrm{CO_2 + H_2O \rightarrow O_2 + CH_2O}$). $\mathrm{O_2}$ is sparingly soluble in water and distributes between the liquid and gas phase according to the Henry's law constant for $\mathrm{O_2}$: $K_{\mathrm{H}} = 1.3 \cdot 10^{-5} \frac{\mathrm{mol}}{\mathrm{m^3 Pa}} = 0.0013 \frac{\mathrm{M}}{\mathrm{atm}}$ at $\mathrm{T} = 298.15\mathrm{K}$ (25°C). The equations for closed system $\mathrm{O_2}$ are as follows:

$$\mathrm{O_{2(total)}} = n_{\mathrm{O_2(g)}} + V_{\mathrm{liquid}} \cdot [\mathrm{O_{2(aq)}}] = \frac{\mathrm{pO_2} \cdot V_{\mathrm{headspace}}}{\mathrm{RT}} + K_{\mathrm{H}} \cdot \mathrm{pO_2} \cdot V_{\mathrm{liquid}}$$

$$\rightarrow \mathrm{pO_2} = \frac{\mathrm{O_{2(total)}}}{\frac{V_{\mathrm{headspace}}}{\mathrm{RT}} + K_{\mathrm{H}} \cdot V_{\mathrm{liquid}}}$$

$\mathrm{pO_2}$ was confirmed at the end of the experiment. Top and bottom figures of panel B (Fig. S7) illustrate the pH and $\mathrm{O_2}$ variations that can result after an inorganic carbon spike. Given these variations, a semi-continuous culture setup with daily headspace sparging was used for main experiments to ensure $\mathrm{CO_2}$ did not run out and $\mathrm{O_2}$ did not build up to inhibitory levels to nitrogenase.

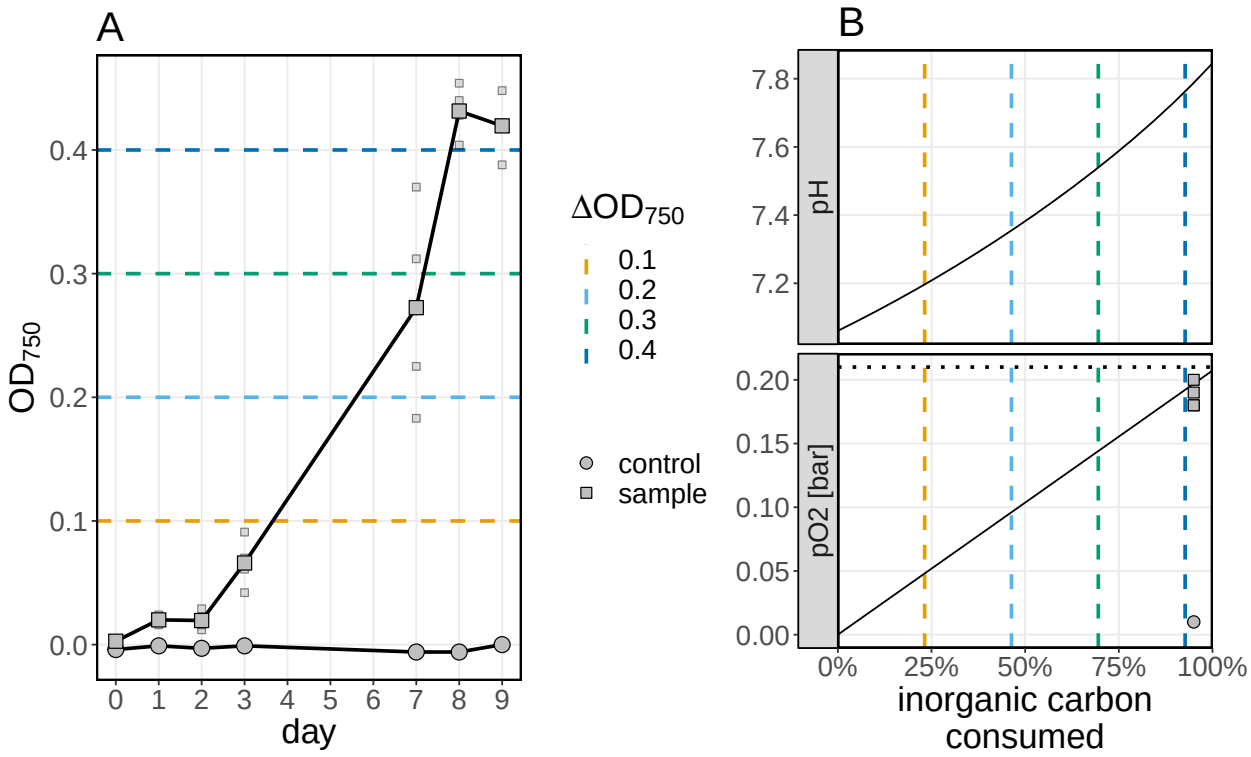

Figure S7: Growth yield, and pH and O_2 variations of *Anabaena cylindrica* cultivated in BG-11_0 under headspace sparged once with 0.5 bar pN_2 and 0.2 bar CO_2. (A) Available carbon sustained culture growth to OD_{750} of ~0.4. (B) pH and pO_2 increased predictably per 0.1 OD_{750} increment as total inorganic carbon was depleted.

Appendix S5: Isotope data and fractionation model

Data

Fig. S8 and Table S5 summarize the measured fractionation factors for *A. cylindrica* and *A. variabilis* from this study. Fig. S9 shows the calibration regressions for correction of raw isotope data.

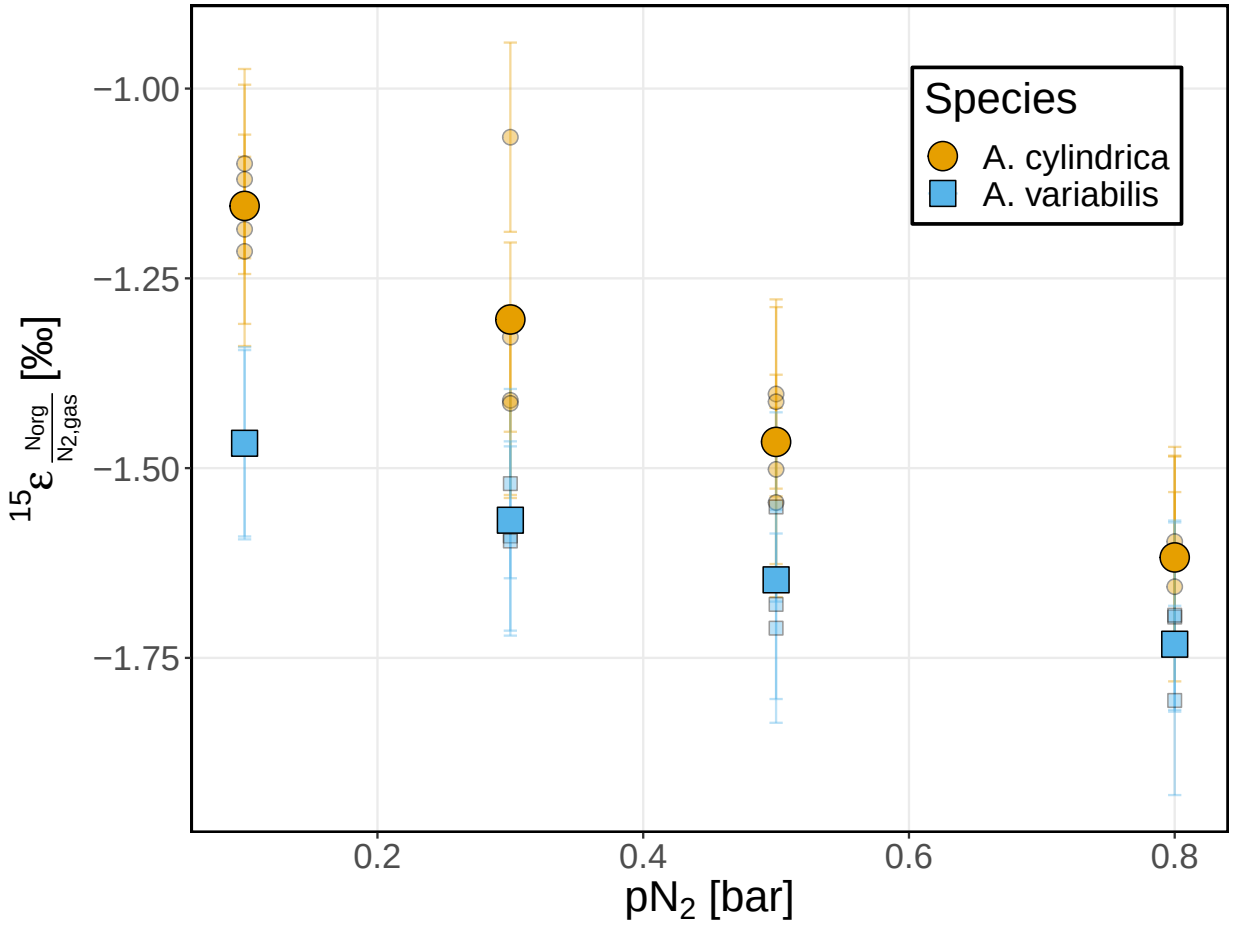

Figure S8: Overview of all biological replicates (small data points) of the isotope fractionation factors (ϵ^{15}N) measured between biomass and N_2 for *Anabaena cylindrica* (circles) and *Anabaena variabilis* (squares) cultivated under different N_2 partial pressures. Large data points represent averages. Error bars show analytical precision (σ_a).

Table S5: Summary of the average isotope fractionation factors (ϵ^{15}N, in ‰ vs. air N_2) between biomass and N_2 from biological replicates of *Anabaena cylindrica* and *Anabaena variabilis* cultivated under different N_2 partial pressures. Reported errors of the means are bootstrapped standard errors (±1 SE). σ_a indicates the analytical precision. The absolute systematic uncertainty on all measurements is 0.3‰ based on the uncertainty of the employed reference material. These data are shown visually in the main text in Fig. 4.

Species	pN_2 [bar]	biological replicates	$\epsilon^{15}N_{Norg/N2.gas}$ [‰]	σ_a [‰]
A. cylindrica	0.1	4	-1.15 ± 0.02	± 0.12
A. cylindrica	0.3	4	-1.31 ± 0.07	± 0.12
A. cylindrica	0.5	4	-1.47 ± 0.03	± 0.12
A. cylindrica	0.8	4	-1.62 ± 0.01	± 0.12
A. variabilis	0.1	2	-1.47 ± 0.00	± 0.12
A. variabilis	0.3	3	-1.57 ± 0.02	± 0.12
A. variabilis	0.5	3	-1.65 ± 0.04	± 0.12
A. variabilis	0.8	3	-1.73 ± 0.03	± 0.12

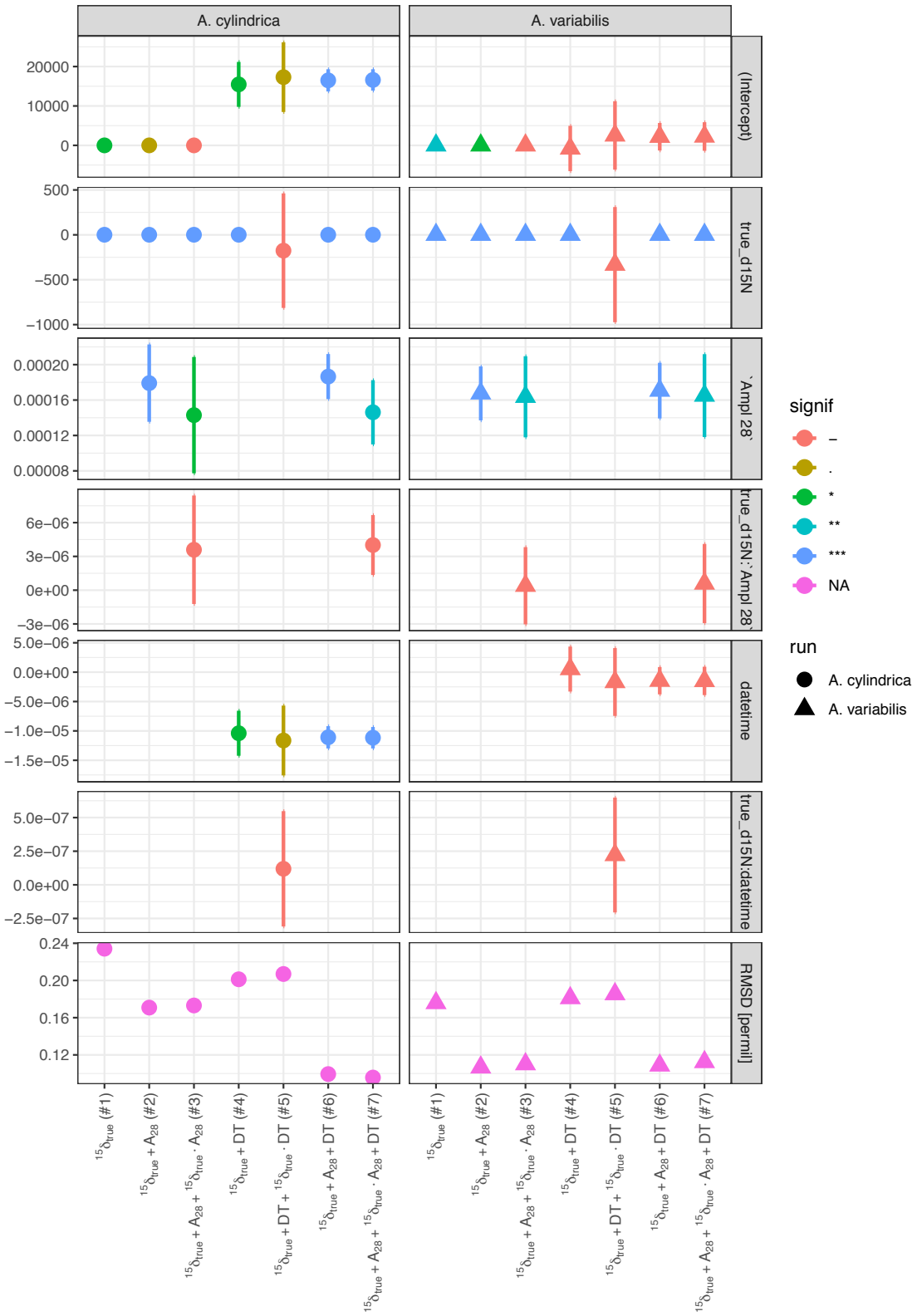

Figure S9: Visualization of calibration regressions for correction of isotope data. Calibration models were run across all isotope standards (detailed in Materials and Methods) evaluating individual parameters to gain a better understanding of their individual contributions and relevance. Regression models tested are numbered across the bottom of the figure and consider the following parameters: isotopic value ($^{15}\delta_{\mathrm{true}}$), signal intensity ($A_{28}$, i.e. amplitude), temporal drift (DT, i.e. datetime), and their cross effects. The simplest combination of parameters that shows statistical significance (i.e. lowest residual mean standard deviation, or RMSD) is the model that best explains the variance in standards (model #6 for *A. cylindrica* (left) and #2 for *A. variabilis* (right), highlighted by the rectangles) and was used to correct the isotopic data.

Isotope fractionation model

This section describes the isotopic flux model used to contextualize the data (as shown in Fig. 7) and provides details on its derivation.

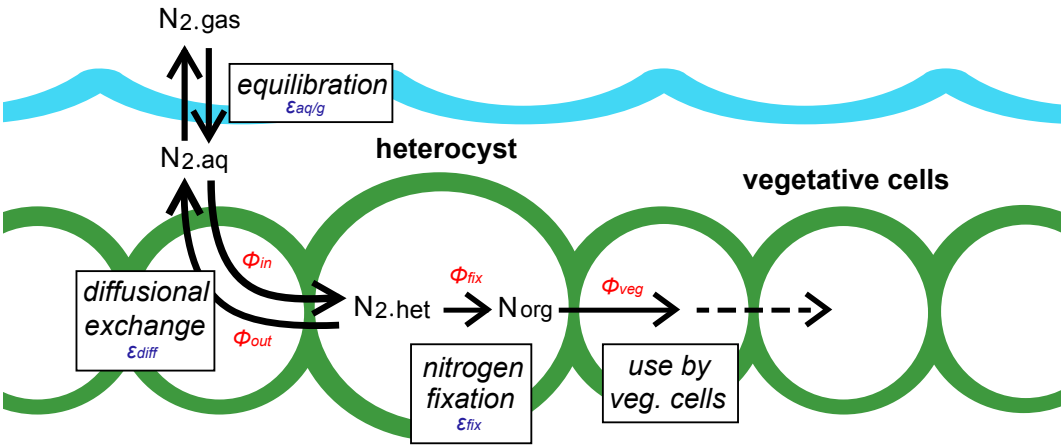

Figure S10: Steady state flux model for the nitrogen isotope fractionation during nitrogen fixation. Same as Fig. 2 with fluxes added in red and fractionation factors in blue for easy reference.

Following the approach employed by Laws et al. (1995) to understand the growth-rate dependent organismal isotope effect during carbon fixation, we developed a quasi steady-state model (Hayes, 2004) for the organismal isotope effect of nitrogen fixation in heterocystous cyanobacterial filaments, as outlined below.

Flux balance

Assuming a quasi steady-state flux of nitrogen through *Anabaena* filaments, N_2 fixed by nitrogenase in the heterocysts (ϕ_{fix}) and delivered to the vegetative cells (ϕ_{veg}) must balance the flux of N_2 in (ϕ_{in}) and out (ϕ_{out}) of the heterocysts. Exchange of N_2 is thought to occur primarily by diffusion through the pores between the vegetative cells and heterocysts (Fig. S10), so the flux of N_2 that enters the heterocyst is proportional to the external concentration of N_2 ($C_{\mathrm{N2.out}}$), while the flux of N_2 that leaves the heterocyst is proportional to the concentration of N_2 within the heterocyst ($C_{\mathrm{N2.het}}$). Dissolved $N_{2.\mathrm{aq}}$ (i.e. $C_{\mathrm{N2.out}}$) is assumed to remain in equilibrium with the virtually infinite reservoir of gaseous $N_{2.\mathrm{gas}}$ ($\mathrm{pN_2}$) in the headspace, with the proportionality between them described by Henry's law ($\mathrm{C_{N2.out}}=K_{\mathrm{H}}\cdot\mathrm{pN_2}$; solubility constant K_{H} for N_2 gas in water is 6.5×10^{-4} mol L^{-1} bar^{-1}, Sander, 2015). This leads to the following set of flux equations:

$$\begin{aligned}
\phi_{\mathrm{veg}} &= \phi_{\mathrm{fix}} \\
\phi_{\mathrm{fix}} &= \phi_{\mathrm{in}} - \phi_{\mathrm{out}} \\
\phi_{\mathrm{out}} &= K_2 \cdot C_{\mathrm{N2.het}} \\
\phi_{\mathrm{in}} &= K_1 \cdot C_{\mathrm{N2.out}} = K_1 \cdot K_{\mathrm{H}} \cdot \mathrm{pN_2}
\end{aligned} \tag{S1}$$

The corresponding isotope flux balances are as follows, with all δ and ϵ values referring to the nitrogen isotope system (errors from mass balance calculations in δ space are assumed to be negligible given the small isotopic

effects; Hayes, 2004):

$$\begin{aligned} \phi_{\text{veg}} \cdot \delta_{\phi\text{veg}} &= \phi_{\text{fix}} \cdot \delta_{\phi\text{fix}} \\ \phi_{\text{fix}} \cdot \delta_{\phi\text{fix}} &= \phi_{\text{in}} \cdot \delta_{\phi\text{in}} - \phi_{\text{out}} \cdot \delta_{\phi\text{out}} \end{aligned} \tag{S2}$$

The isotopic composition of the fluxes ($\delta_{\phi\text{x}}$) can be described as follows, with $\epsilon_{\text{aq/g}}$ as the equilibrium fractionation factor between the aqueous and gaseous phase of N_2; ϵ_{diff} the kinetic isotope fractionation factor of N_2 diffusion through the aqueous medium and cells; and ϵ_{fix} the intrinsic kinetic isotope fractionation factor of nitrogenase during the nitrogen fixation reaction (see Fig. S10 for visualization of the fluxes and reservoirs):

$$\begin{aligned} \delta_{\phi\text{veg}} &= \delta_{\text{Norg}} \\ \delta_{\phi\text{fix}} &= \delta_{\text{N2.het}} - \varepsilon_{\text{fix}} \\ \delta_{\phi\text{out}} &= \delta_{\text{N2.het}} - \varepsilon_{\text{diff}} \\ \delta_{\phi\text{in}} &= \delta_{\text{N2.gas}} + \varepsilon_{\frac{\text{aq}}{g}} - \varepsilon_{\text{diff}} \end{aligned} \tag{S3}$$

All kinetic fractionation factors are defined as ${}^{15}\epsilon_{\frac{\text{Norg}}{\text{N2.gas}}} = \left[\left(\frac{{}^{15}\text{N}}{{}^{14}\text{N}} \right)_{\text{N}_{\text{org}}} / \left(\frac{{}^{15}\text{N}}{{}^{14}\text{N}} \right)_{\text{N}_{\text{2.gas}}} - 1 \right] \times 1000$ as discussed in the Materials and Methods. As indicated by Eq. S3, the isotopic composition of the N_2 entering the heterocyst ($\delta_{\phi_{\text{in}}}$) depends on the isotopic composition of the gaseous N_2 in the headspace or atmosphere ($\delta_{\text{N2.gas}}$) in equilibrium with the aqueous N_2 reservoir, $\epsilon_{\text{aq/g}}$ and ϵ_{diff}; the isotopic composition of the fixed nitrogen ($\delta_{\phi_{\text{fix}}}$) depends on the isotopic composition of N_2 inside the heterocyst ($\delta_{\text{N2.het}}$) and ϵ_{fix}. The isotopic composition of the N_2 exiting the heterocyst ($\delta_{\phi_{\text{out}}}$) depends on $\delta_{\text{N2.het}}$ and ϵ_{diff}. Combining Eqs. S1, S2 and S3 leads to the following expression for the overall organismal fractionation factor between organic nitrogen and N_2 gas ($\varepsilon_{\text{Norg/N2.gas}}$):

$$\varepsilon_{\frac{\text{Norg}}{\text{N2.gas}}} = \delta_{\text{Norg}} - \delta_{\text{N2.gas}} = \varepsilon_{\frac{\text{aq}}{g}} - \varepsilon_{\text{diff}} + (\varepsilon_{\text{diff}} - \varepsilon_{\text{fix}}) \frac{K_2 \cdot C_{\text{N2.het}}}{K_1 \cdot K_{\text{H}} \cdot \text{pN}_2} \tag{S4}$$

Growth constraints

Because nitrogen is the sole limiting nutrient in this system, the steady-state growth rate (μ) of the vegetative cells ($\mu \cdot n_{veg}$) must be proportional to the total flux of nitrogen fixed ($\phi_{\text{fix.total}}$). In the case of *A. cylindrica*, nitrogen fixation is confined to the heterocysts, so $\phi_{\text{fix.total}}$ can be inferred from the number of heterocysts (n_{het}) and the average nitrogen fixation flux per heterocyst (ϕ_{fix}), leading to the following set of equations (with yield constant K_{Y} for biomass growth):

$$\begin{aligned} \phi_{\text{fix.total}} &= \phi_{\text{fix}} \cdot n_{\text{het}} \\ \mu \cdot n_{\text{veg}} &= K_{\text{Y}} \cdot \phi_{\text{fix.total}} = K_{\text{Y}} \cdot \phi_{\text{fix}} \cdot n_{\text{het}} \end{aligned} \tag{S5}$$

The ratio of vegetative to heterocyst cells ($\frac{n_{\text{veg}}}{n_{\text{het}}}$) can be more intuitively represented as the *number of vegetative cells between heterocysts* (n_{cbh}), which is used to represent data for the heterocyst intervals (see Figs. 4 and S2). Combining Eq. S5 with the fluxes from Eq. S1 to eliminate ϕ_{fix} gives the following expression:

$$\mu = K_{\text{Y}} \cdot \frac{K_1 \cdot K_{\text{H}} \cdot \text{pN}_2 - K_2 \cdot C_{\text{N2.het}}}{n_{\text{cbh}}} \tag{S6}$$

Eq. S6 can be combined with Eq. S4 to eliminate $C_{\mathrm{N2.het}}$ and yield the following expression for $\varepsilon_{\mathrm{Norg/N2.gas}}$:

$$\varepsilon_{\frac{\mathrm{Norg}}{\mathrm{N2.gas}}} = \varepsilon_{\frac{\mathrm{aq}}{g}} - \varepsilon_{\mathrm{diff}} - (\varepsilon_{\mathrm{diff}} - \varepsilon_{\mathrm{fix}}) \left(1 - \frac{1}{K_1 \cdot K_{\mathrm{Y}} \cdot K_{\mathrm{H}}} \cdot \frac{\mu \cdot n_{\mathrm{cbh}}}{\mathrm{pN_2}}\right) \tag{S7}$$

With the isotope effects of N_2 diffusion through water assumed to be negligible ($\epsilon_{\mathrm{diff}} \approx 0‰$), Eq. S7 can be simplified to the following final equation:

$$\varepsilon_{\frac{\mathrm{Norg}}{\mathrm{N2.gas}}} = \varepsilon_{\frac{\mathrm{aq}}{g}} - \varepsilon_{\mathrm{fix}} + \frac{\varepsilon_{\mathrm{fix}}}{K_1 \cdot K_{\mathrm{Y}} \cdot K_{\mathrm{H}}} \cdot \frac{\mu \cdot n_{\mathrm{cbh}}}{\mathrm{pN_2}} \tag{S8}$$

Eq. S8 was used to estimate the fractionation factor of nitrogenase ($\epsilon_{\mathrm{fix}} = -2.71 \pm 0.09‰$; Fig. 7) based on heterocyst spacing (Fig. 4), growth rate (Fig. S6) and isotopic data (Fig. 5) of *A. cylindrica* from this study, as well as literature data on $\epsilon_{\mathrm{aq/g}}$ (Fig. S11). To our knowledge, this is the first *in vivo* estimate of ϵ_{fix} for nitrogenase.

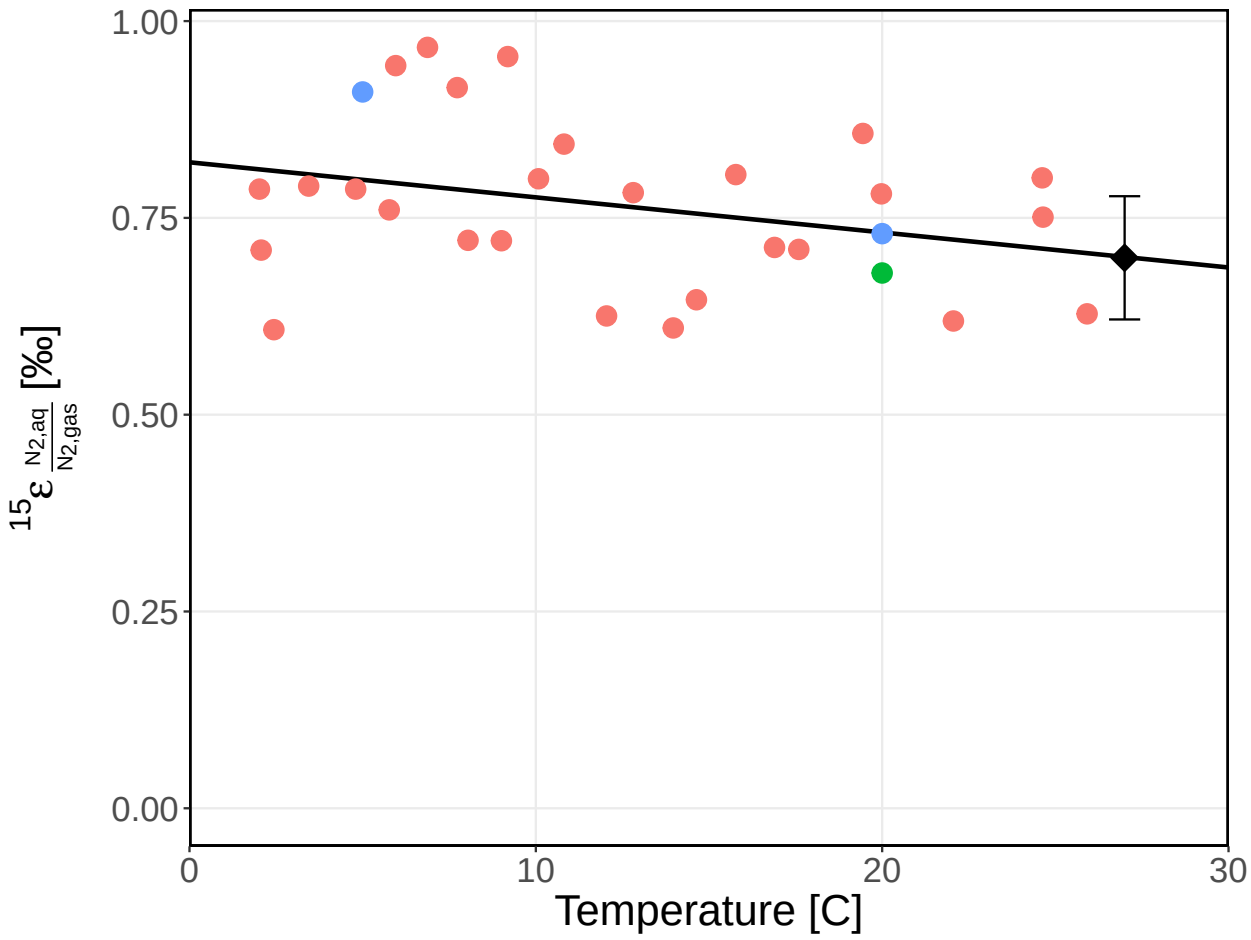

Figure S11: Temperature dependence of the equilibrium fractionation between atmospheric/headspace N_2 gas and dissolved/aqueous N_2. Diamond indicates the predicted fractionation factor ($\epsilon_{\mathrm{aq/g}} = 0.70 \pm 0.08‰$) at the growth temperature used in this study (27°C). Red data points are digitized from Fig. 1 in Klots and Benson, 1963; blue data points from Table 1 in Lee et al., 2015; and green data point from Table 1 in Knox et al., 1992.

Appendix S6: Enzyme kinetics model

In addition to its role in overall flux balance and as a constraint on growth rate, the nitrogen fixation flux inside a heterocyst (ϕ_{fix}) can also be expressed with respect to the substrate-dependent rate of enzymatic catalysis with Michaelis-Menten parameters $V_{\max}$ (the maximum rate of catalysis) and K_{M} (the half-saturation constant):

$$\phi_{\text{fix}} = V_{\max} \cdot \frac{C_{\text{N2.het}}}{C_{\text{N2.het}} + K_{\text{M}}} \tag{S1}$$

Combining this equation with the growth-rate dependent flux expression derived in Eq. S5 from Appendix S5: (where $\frac{n_{\text{veg}}}{n_{\text{het}}} = n_{\text{cbh}}$) yields:

$$\frac{\mu \cdot n_{\text{cbh}}}{K_{\text{Y}}} = V_{\max} \cdot \frac{C_{\text{N2.het}}}{C_{\text{N2.het}} + K_{\text{M}}} \tag{S2}$$

which can be solved for n_{cbh}:

$$n_{\text{cbh}} = \frac{K_{\text{Y}} V_{\max}}{\mu} \cdot \frac{C_{\text{N2.het}}}{C_{\text{N2.het}} + K_{\text{M}}} \tag{S3}$$

Eliminating $C_{\text{N2.het}}$ with Eq. S4 from Appendix S5: finally yields:

$$n_{\text{cbh}} = K_{\text{Y}} \cdot V_{\max} \cdot \frac{\text{pN}_2}{\mu} \cdot \frac{1}{\text{pN}_2 + \frac{\varepsilon_{\text{fix}}}{\varepsilon_{\frac{\text{aq}}{\text{g}}} - \varepsilon_{\frac{\text{Norg}}{\text{N2.gas}}}} \cdot \frac{K_{\text{M}}}{K_{\text{H}}}} \tag{S4}$$

Bootstrapped non-linear least squares regression fitting of Eq. S4 based on the heterocyst spacing (Fig. 4), growth rate (Fig. S6) and isotopic data (Fig. 5) from this study provides an estimate of the Michaelis-Menten half-saturation constant K_{M} (or to be precise, $K_{\text{M}}/K_{\text{H}}$, the half-saturation constant in pressure instead of concentration units) for nitrogenase in each phase of *A. cylindrica* culture growth (as reported in the discussion section of the main text). Our estimates fall within the scope of other literature estimates for nitrogenase (Table S6).

Table S6: Overview of Michaelis-Menten half-saturation constants for N_2 fixation by intact cells (IC) and cell-free extracts (CFX). K_{M} values reported for this study are separated by culture growth phase.

Organism	Type	K_{M} [bar N_2]	Reference
Anabaena cylindrica (early-exponential)	IC	0.12	This study
Anabaena cylindrica (late-exponential)	IC	0.12	This study
Anabaena cylindrica	IC	0.20	Ohmori and Hattori, 1972
Anabaena variabilis	IC	0.12	Jensen and Raymond, 1983
Azotobacter vinelandii	IC	0.12	Hwang and Burris, 1972
Azotobacter vinelandii	CFX	0.16	Strandberg and Wilson, 1967
Azotobacter vinelandii	CFX	0.16	Hardy and Jr. Knight, 1967

Appendix S7: References

Hardy, R. W. F., Jr. Knight, E., 1967. ATP-dependent reduction of azide and HCN by N_2-fixing enzymes of *Azotobacter vinelandii* and *Clostridium pasteurianum*. Biochimica et Biophysica Acta 139, 69–90.

Hayes, J. M., 2004. An introduction to isotopic calculations. Atomic Energy, 1–10.

Hwang, J. C., Burris, R. H., 1972. Nitrogenase-catalyzed reactions. Biochimica et Biophysica Acta 283, 339–350.

Jensen, B. B., Raymond, R. P., 1983. Direct measurements of steady-state kinetics of cyanobacterial N_2 uptake by membrane-leak mass-spectrometry and comparisons between nitrogen-fixation and acetylene-reduction. Applied and Environmental Microbiology 45, 1331–1337.

Klots, C. E., Benson, B. B., 1963. Isotope effect in solution of oxygen and nitrogen in distilled water. Journal of Chemical Physics 38, 890–892.

Knox, M., Quay, P. D., Wilbur, D., Dec. 1992. Kinetic isotopic fractionation during air-water gas transfer of O_2, N_2, CH_4, and H_2 97, 20335–20343.

Laws, E. A., Popp, B. N., Bidigare, R. R., Kennicutt, M. C., Macko, S. A., 1995. Dependence of phytoplankton carbon isotopic composition on growth rate and $[CO_2]_{aq}$: Theoretical considerations and experimental results. Geochimica et Cosmochimica Acta 59, 1131–1138.

Lee, H., Sharp, Z. D., Fischer, T. P., 2015. Kinetic nitrogen isotope fractionation between air and dissolved N_2 in water: Implications for hydrothermal systems. Geochemical Journal 49, 571–573.

Ohmori, M., Hattori, A., 1972. Effect of nitrate on nitrogen-fixation by the blue-green alga *Anabaena cylindrica*. Plant and Cell Physiology 13, 589–599.

Sander, R., 2015. Compilation of Henry's law constants (version 4.0) for water as solvent. Atmospheric Chemistry and Physics 15, 4399–4981.

Strandberg, G. W., Wilson, P. W., 1967. Molecular H_2 and the pN_2 function of *Azotobacter*. Proceedings of the National Academy of Sciences of the United States of America 58, 1404–1409.